Monthly Notices of the ROYAL ASTRONOMICAL SOCIETY

MNRAS **519,** 2929–2939 (2023)
Advance Access publication 2022 December 9

https://doi.org/10.1093/mnras/stac3606

# Low-redshift quasars in the SDSS Stripe 82 – III. MOS observations

D. Bettoni [1]★ R. Falomo [1]★ S. Paiano [2] J. K. Kotilainen[3,4] and M. B. Stone [3,4]

[1]*INAF–Osservatorio Astronomico di Padova, Vicolo dell'Osservatorio 5, I-35122 Padova (PD), Italy*
[2]*INAF–IASF Palermo, via Ugo La Malfa 153, I-90146 Palermo, Italy*
[3]*Finnish Centre for Astronomy with ESO (FINCA), University of Turku, FI-20014 Turku, Finland*
[4]*Department of Physics and Astronomy, University of Turku, FI-20014 Turku, Finland*

Accepted 2022 December 4. Received 2022 November 25; in original form 2022 July 1

## ABSTRACT

We present multi-object optical spectroscopy of the galaxies in the environment of 12 low-redshift ($z < 0.5$) quasars and of 11 inactive massive galaxies chosen to match the properties of the quasar host galaxies to probe physical association and possible events of recent star formation (SF). The quasars are selected from a sample of QSOs in the Sloan Digital Sky Survey (SDSS) Stripe 82 region for which both the host galaxy and the large-scale environments were previously investigated. The new observations complement those reported in our previous works on close companion galaxies of nearby quasars. For the whole data set, we find that for about half (19 out of 44) of the observed QSOs, there is at least one associated companion galaxy. In addition to the new spectroscopic observations, we add data from the SDSS data base for the full sample of objects. We find that the incidence of companion galaxies in the fields of QSO (17 per cent) is not significantly different from that of inactive galaxies (19 per cent) similar to quasar hosts in redshift and mass. Nevertheless, the companions of quasars exhibit more frequently emission lines than those of inactive galaxies, suggesting a moderate link between the nuclear activity and recent SF in their environments.

**Key words:** galaxies: active – galaxies: evolution – galaxies: nuclei – *(galaxies)* quasars: general.

## 1 INTRODUCTION

The nuclear activity in quasars is assumed to occur due to a major merger of two gas-rich galaxies that feed the central engine and enable the growth of a stellar spheroid. However, details on what triggers the gas fuelling and how nuclear activity affects the subsequent evolution of the host galaxies remain not fully understood. The correlations observed between the black hole (BH) mass ($M_{\rm BH}$) and the properties of the associated galaxy bulge as the $M_{\rm BH}$–$\sigma_{\rm stars}$ (Ferrarese & Merritt 2000) or $M_{\rm BH}$–$M^{*}_{\rm bulge}$ (Kormendy & Ho 2013) seem to point to a co-evolution of BH and spheroids, but it did not yet clarify the role played by the environment, which is a fundamental component in investigating issues of quasar activity and its role in the evolution of galaxies. Minor and major mergers may have a key role for triggering and fuelling the nuclear activity. The global properties of the galaxy environment are probably the main driver of the active galactic nucleus (AGN) activity (i.e. Kauffmann & Haehnelt 2000; Di Matteo, Springel & Hernquist 2005).

However, the role of the environment on nuclear activity is still a puzzling subject; in fact, it is relevant to constrain processes that trigger and control activity and also to investigate its relationship to star formation (SF). For example, the relationship of galaxy environment with SF and/or morphology may not be universal (e.g. Wijesinghe et al. 2012).

Looking at the environment at Mpc scales, comparing that of quasars to those of galaxies has given conflicting results partially due to limited samples and lack of homogeneous data sets. Early studies on the galaxy environments suggest that quasars are more strongly clustered than galaxies (e.g. Shanks, Tanvir & Redfern 1988), while later studies based on surveys, such as the Two Degree Field Survey and the Sloan Digital Sky Survey (SDSS), found galaxy densities around quasars and inactive galaxies (ING) to be comparable to each other (e.g. Smith et al. 2000; Wake et al. 2004). Using the SDSS archives, Serber et al. (2006) and Strand, Brunner & Myers (2008) have taken advantage of the large data sets provided by the survey to study quasars at $z < 0.4$. Both studies found that quasars are located in higher local overdensity regions than typical L* galaxies, and that density enhancement is strongest within 100 kpc from the quasar. Serber et al. (2006) also found that high-luminosity quasars have denser small-scale environments than QSOs at lower luminosity. This result was pointed out also by Shen et al. (2009), who find that at $z < 2.5$, 10 per cent of the most optically luminous quasars are more strongly clustered. More recently, Stott et al. (2020) found that ultraviolet-bright QSOs in the same range of redshift are found to be in overdense regions. In spite of these studies, our knowledge of the physical association of the galaxies around low-$z$ QSO and their dynamical properties still remains poor. However, Karhunen et al. (2014) finds that the number density of galaxies in a projected volume of 1 Mpc radius for a sample of QSO ($z < 0.5$) and a comparison sample of passive galaxies matched in luminosity with the host galaxy of the QSO is very similar. More recently, Wethers et al. (2022) analysing data from the Galaxy and Mass Assembly (GAMA) survey found again that QSO activity weakly depends on

★ E-mail: daniela.bettoni@oapd.inaf.it (DB); renato.falomo@inaf.it (RF)

the galaxy environment both on large (Mpc) and small (<100 kpc) scales.

In the past years, a series of papers (Falomo et al. 2014; Karhunen et al. 2014; Bettoni et al. 2015) studied the host galaxy properties, environment, and SF for a large (∼400) sample of low-redshift ($z < 0.5$) quasars in the SDSS Stripe 82 area. In particular, with regard to the environment, Karhunen et al. (2014) found that quasars are on average found associated with small group of galaxies. The overdensities of galaxies are mainly observed in the closest (<200 kpc) region around the source and vanish beyond a distance of 1 Mpc. The crucial test for this result is the spectroscopic study of the galaxies in the closest volume. We have recently completed a long-slit spectroscopic study [Bettoni et al. 2017 (hereafter Paper I); Stone et al. 2021 (hereafter Paper II)] for 34 QSOs in which we found that ∼44 per cent have at least one associated galaxy. We found that many of the associated companions and some host galaxies exhibit episodes of (recent) SF possibly induced by past interactions (Paper II). The star formation rate (SFR) of the companion galaxies is, however, modest, and the role of the quasar remains uncertain. The long-slit spectroscopy, of course, gets an incomplete view of the environment being limited to the very close companions and is very telescope time expensive. Here, we extend the sample in order to gain statistical significance and thanks to the Multi Object Spectroscopy (MOS) observations to gain a more complete view of the close environment. In addition, in this paper, we add a further crucial step of obtaining similar data for ING well matched in redshift and galaxy luminosity to the quasar hosts.

This paper is organized as follows. The data sample is presented in Section 2 and the analysis in Section 3. The results of this study and an overview including findings from Paper I and Paper II are presented in Section 4. Finally, in Section 5, we summarize our main conclusions. The results are obtained in the framework of the concordance cosmology, using $H_0 = 70$ km s$^{-1}$ Mpc$^{-1}$, $\Omega_m = 0.3$, $\Omega_\lambda = 0.7$.

## 2 THE SAMPLE

We obtained spectra of the objects in the fields of 12 QSOs and 11 ING. The QSO targets were selected from the Falomo et al. (2014) parent sample of 416 low-redshift QSOs located in the Stripe 82 (Annis et al. 2014) region of the sky for which complete information was provided concerning the characterization of the host galaxy and their galaxy environments. The QSO targets for this study were selected on the basis of good observability and feasibility from the adopted instrumentation. The selected fields are also chosen among objects well resolved [in Falomo et al. (2014) objects defined as *resolved*] in order to study the possible connection between host and associated companions and events of recent SF. For each field, the number of possible observed companions was limited to 8–11, as to not overlap slitlets on the MOS plate (see also Section 3). For the comparison sample of ING, we selected the targets from the study of 580 passive galaxies by Karhunen et al. (2014). This control sample of galaxies has the same redshift distribution of the QSO sample. Moreover, we also matched the galaxy absolute magnitude to that of the host galaxy of the resolved QSO [see Falomo et al. (2014) for details]. The average redshift is $z = <0.31> \pm 0.04$ and $z = <0.32> \pm 0.05$ for QSOs and ING, respectively, and the average absolute magnitude $M_r = <-22.72> \pm 0.24$ and $M_r = <-22.49> \pm 0.22$ (see also Fig. 1).

The two samples are also comparable in terms of large-scale environment properties (Karhunen et al. 2014). The galaxy number density within 0.25 Mpc is 7.1 ± 2 for QSOs and 7.0 ± 3 for ING.

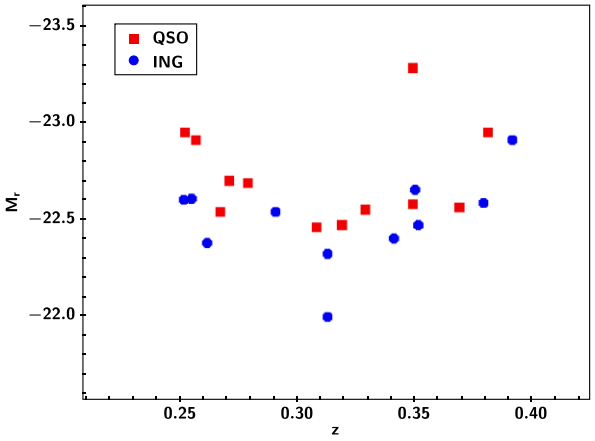


**Figure 1.** Scatter plot of the absolute *r* magnitude as a function of the redshift of the QSO host galaxies and of the ING.

**Table 1.** Observed QSO fields.

| Nr | RA 2000 | Dec. 2000 | $z$ | $M_r$ (nuc) | $M_r$ (host) | $N_{slit}$ |
|---|---|---|---|---|---|---|
| 16 | 312.4859 | −0.20048 | 0.3693 | −24.5 | −22.56 | 4 |
| 62 | 329.4341 | 0.88434 | 0.2674 | −22.23 | −22.54 | 5 |
| 68 | 329.95421 | 0.16799 | 0.2713 | −22.93 | −22.7 | 5 |
| 127 | 348.21203 | 0.28862 | 0.257 | −22.41 | −22.91 | 7 |
| 147 | 355.42293 | −0.63519 | 0.319 | −23.85 | −22.47 | 4 |
| 154 | 357.38655 | −0.61273 | 0.279 | −23.63 | −22.69 | 4 |
| 192 | 7.13215 | −0.07036 | 0.2519 | −23.03 | −22.95 | 16 |
| 195 | 8.63226 | −0.2202 | 0.3811 | −23.51 | −22.95 | 6 |
| 204 | 10.5561 | 0.98825 | 0.3289 | −22.95 | −22.55 | 4 |
| 205 | 10.83224 | 0.85429 | 0.3083 | −23.28 | −22.46 | 10 |
| 239 | 20.21226 | −0.30916 | 0.49 | −22.9 | −23.28 | 15 |
| 270 | 28.16225 | 0.15987 | 0.3492 | −23.2 | −22.58 | 8 |

*Notes.* Column 1: catalogue identification number from Falomo et al. (2014). Column 2: object RA. Column 3: object Dec. Column 4: redshift. Columns 5 and 6: k-corrected absolute *r* magnitude of the QSO and of the host galaxy. Column 7: number of used slits in the field.

**Table 2.** Observed ING fields.

| Nr | RA 2000 | Dec. 2000 | $z$ | $M_r$ | $N_{slit}$ |
|---|---|---|---|---|---|
| 32 | 6.13655 | 0.136926 | 0.3793 | −22.58 | 4 |
| 35 | 7.256614 | −0.47575 | 0.2906 | −22.54 | 5 |
| 45 | 10.18925 | 0.14944 | 0.313 | −22.32 | 2 |
| 55 | 12.601671 | −0.381672 | 0.2517 | 22.60 | 5 |
| 76 | 16.32155 | 0.898009 | 0.2616 | −22.38 | 9 |
| 77 | 16.4306 | 0.8878843 | 0.3516 | −22.47 | 4 |
| 80 | 16.54892 | −0.3190616 | 0.3516 | −21.40 | 4 |
| 81 | 16.55616 | 0.9371725 | 0.3913 | −22.91 | 4 |
| 120 | 16.55616 | 0.9371725 | 0.3913 | −22.00 | 2 |
| 514 | 337.48396 | 0.070315 | 0.2549 | −22.61 | 5 |
| 548 | 350.21705 | −0.301583 | 0.3499 | −22.66 | 9 |

*Notes.* Column 1: catalogue identification number from Karhunen et al. (2014). Column 2: object RA. Column 3: object Dec. Column 4: redshift. Column 5: k-corrected absolute *r* magnitude. Column 6: number of used slits in the field.

The lists of the observed quasar and ING fields are given in Tables 1 and 2, respectively.

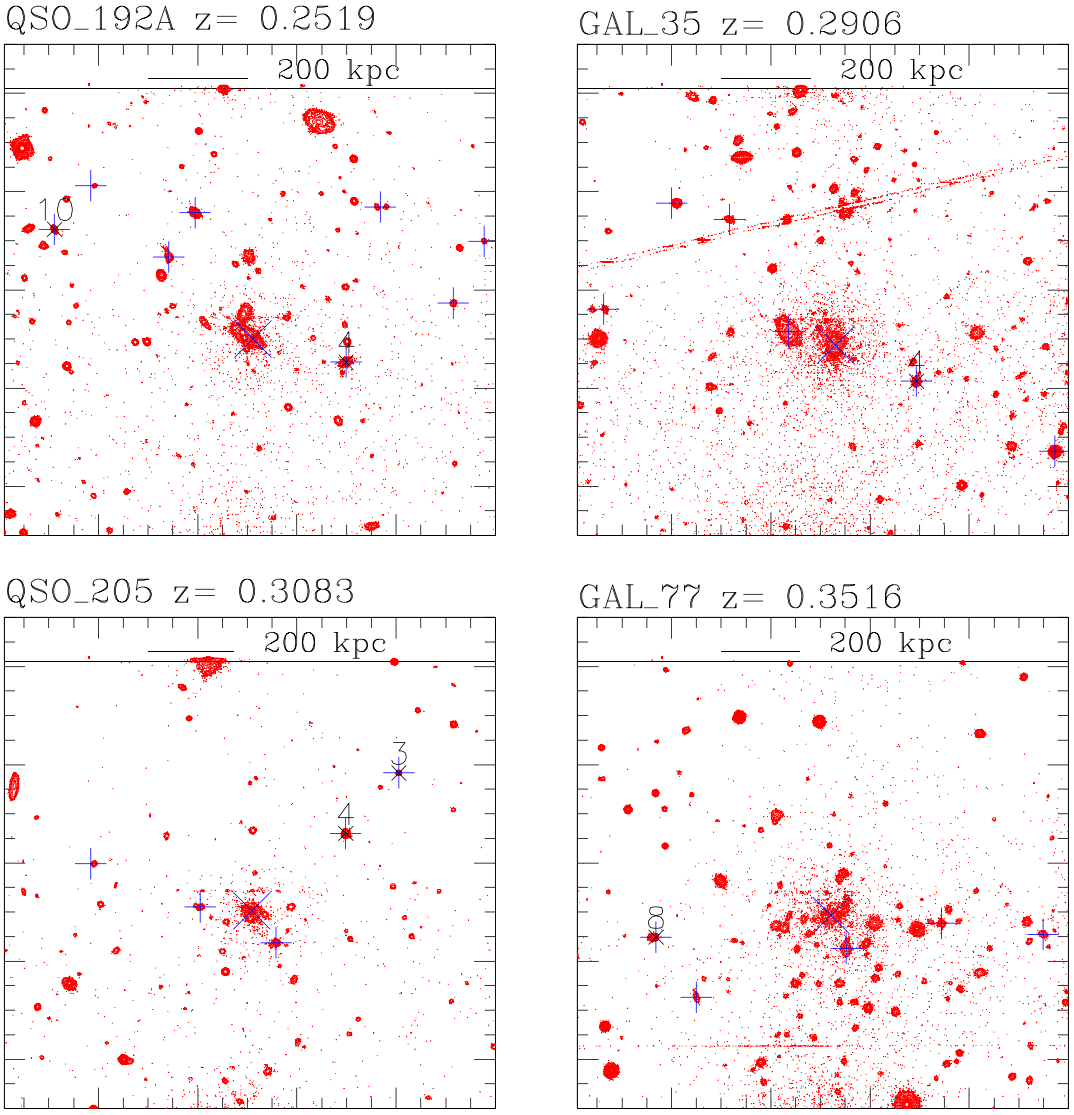


**Figure 2.** *r*-band contour plot of observed QSO and ING fields. The numbers of QSO and galaxies refer to objects in Falomo et al. (2014) and Karhunen et al. (2014). The large blue X in the centre indicates the target. Companion galaxies are labelled by a star and the slit number. The other slits observed are marked with blue crosses. Only the slits for the spectra with enough S/N are plotted. The top bar shows a scale of 200 kpc at the redshift of the target. North is up and East to the right.

## 3 OBSERVATIONS AND DATA ANALYSIS

The optical spectroscopy for the galaxies in the 23 fields was secured with the European Southern Observatory (ESO) Faint Object Spectrograph and Camera (EFOSC2) in MOS mode at the ESO New Technology Telescope, covering the spectral range 3800–9000 Å. We adopted the grism #4 and a PunchHead slit width of 1.34 arcsec, yielding an effective spectral resolution corresponding to a full width at half-maximum of ∼20 Å. The observations were carried out in two observing runs in 2019: the first from August 28 to September 3 and the second from October 3 to 8. During the first observing night, all the fields were observed in pre-imaging with *r* filter with an average observing time of 20 min. These images were used to select the targets in each field for the subsequent MOS spectroscopic observations. For each field, therefore, a slit mask of up to 10 slits of ∼8.6 arcsec length was produced. The average brightness in *r* band for the companion galaxy candidate in the fields is in the range of ∼19.5–21.5. For each field, we first chose the slits for the brightest targets and then, depending on the constraint on the MOS-slit positions, we selected fainter objects in order to fill all the available slits and to secure that slitlets do not overlap on the MOS plate. The constraints on the MOS-slit positions in some cases forced us to place the slit at the faint targets. For the 23 fields, we used ∼230 slit positions. Given the above conditions, in a number of cases, the spectra resulted with insufficient signal-to-noise (S/N) ratio to perform reliable measurements. The same conditions were applied both for QSO fields and ING fields.

For each MOS configuration, we obtained three exposures for a total integration time of 1 h. For three QSO fields (Nr 192, 205, and 239), two different MOS configurations were secured in order to optimize the selection of targets in these fields. In Figs 2 and 3, we show the isophotal contours of the fields of the QSOs and ING for which we found companions.

All the reduction steps were performed using the ESOREFLEX package (Freudling et al. 2013). This includes flat-fielding, wavelength calibration, and background subtraction. Multiple exposures

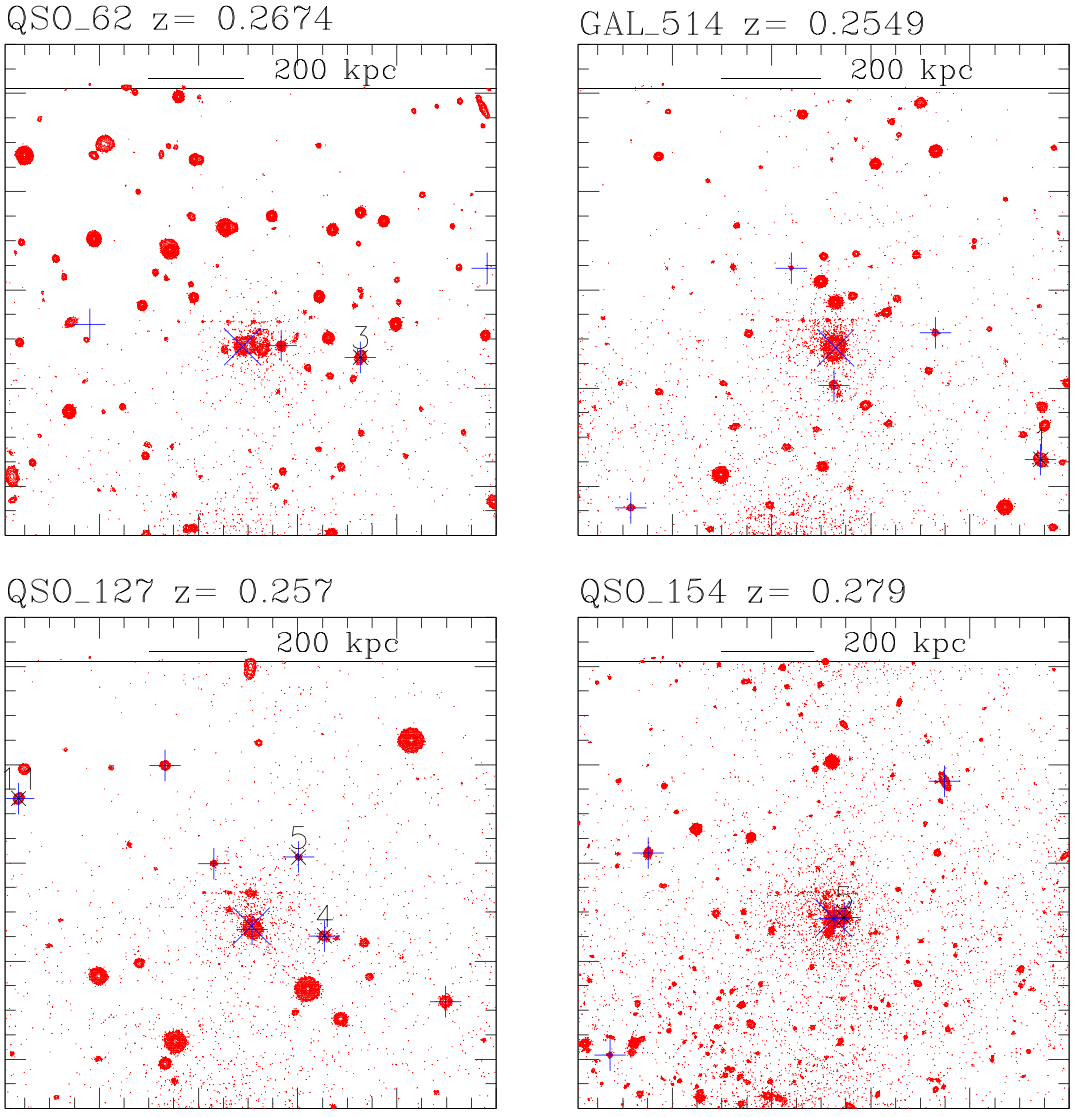


**Figure 3.** *r*-band contour plot of observed quasar and ING fields. The numbers of QSO and galaxies refer to objects in Falomo et al. (2014) and Karhunen et al. (2014). The large blue X in the centre indicates the target. Companion galaxies are labelled by a star and the slit number. The other slits observed are marked with blue crosses. Only the slits for the spectra with enough S/N are plotted. The top bar shows a scale of 200 kpc at the redshift of the target. North is up and East to the right.

were combined with cosmic ray rejection option in order to clean the frames. The resulting accuracy of the wavelength calibration is 0.2 Å. The 1D spectra were then extracted from the 2D background subtracted frames and calibrated for the relative sensitivity of the instrument using spectra of spectrophotometric standard stars observed during the same run. Finally, since the use of a narrow slit might lose a fraction of the light of the companion galaxies, we flux calibrated the spectra in absolute flux using the magnitude of the galaxies derived from SDSS data base.

As a first step, we inspected all the final 1D extracted spectra and keep for measurement only those with average S/N $>$ 5. The redshift was derived using the RVSAO package (Kurtz & Mink 1998): the EMSAO routine in the cases where emission lines are present and XCSAO one for pure absorption spectra. For the XCSAO star from the Jacoby, Hunter & Christian ( 1984) stellar library. Only spectra achieving a correlation factor *r* (Kurtz & Mink 1998) higher than 2 have been considered reliable. A further visual check was also performed. Since the correlation peak can be related to the measurement error, we estimate an average error for our measured redshift of $\sim$80 km s$^{-1}$. In 14 cases, the obtained spectra turned out to be stars and were therefore discarded. At the end of this cleaning, we were able to measure a reliable redshift for 129 objects.

## 4 RESULTS

We are able to secure optical spectra of galaxies in the fields around 23 targets. For 12 quasar fields, we measured 76 spectra and for the 11 fields around massive ING, we gathered 53 spectra. In Figs 4 and 5, we show for two QSOs and two ING the spectra of both the QSO/ING and their companion galaxy. The properties of all observed galaxies are reported in Table A1. We consider that an object is associated with the QSO/ING if the difference in velocity is $\Delta V < 1000$ km s$^{-1}$. This choice represents a compromise between smaller velocity difference that ensures higher confidence of physical association but reduces the statistics and larger values that reduce the confidence but allow for better statistics. Note also that in most cases the redshift of the quasar

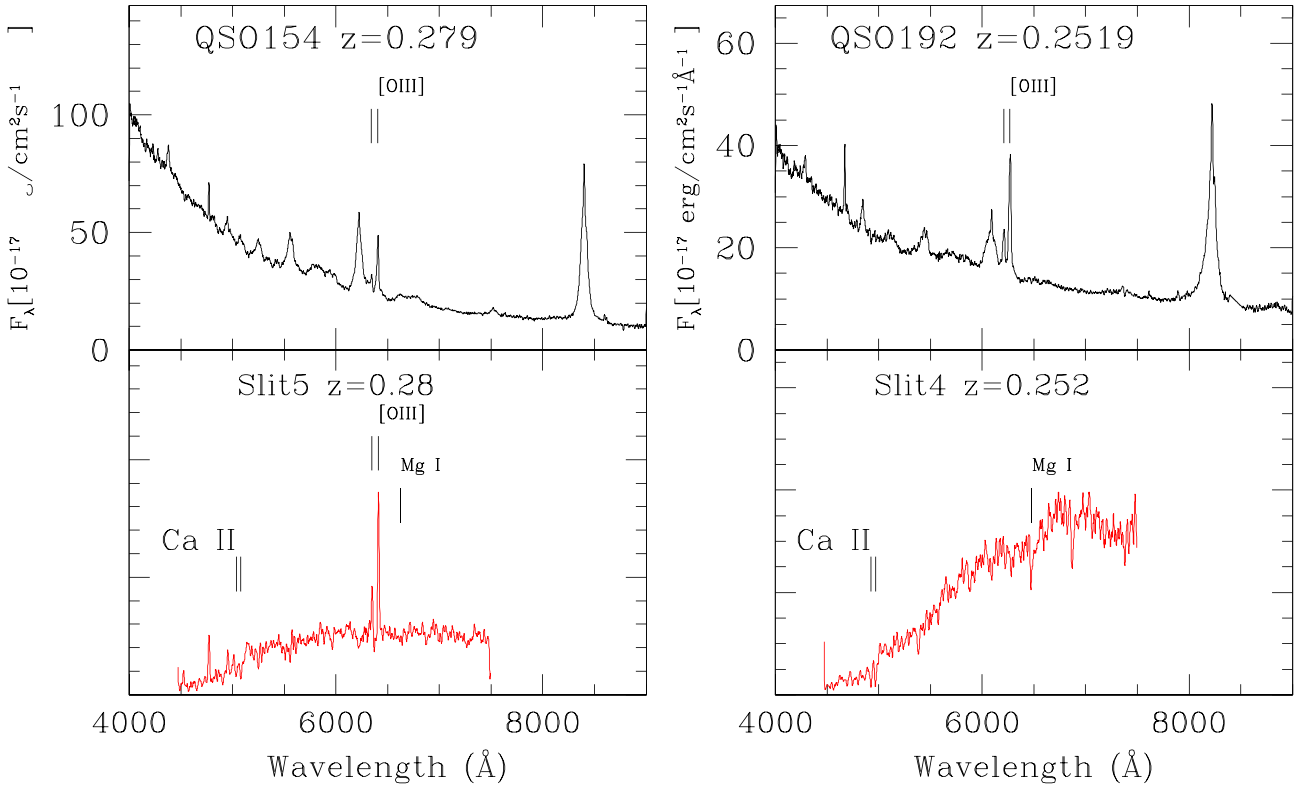


**Figure 4.** Examples of the optical spectrum of QSO (top panels) from SDSS DR16 and its companion galaxy (bottom panels) from this work. QSO numbers are from Falomo et al. (2014).

is based (by SDSS pipeline) on all emission lines including broad lines and thus possibly biased by 500 km s$^{-1}$ and more with respect to the systemic velocity. The relative velocity difference cut-off limit is imposed to reasonably minimize the contamination by chance projection of companions, which are not gravitationally bound while maintaining sufficient pair statistics (Patton et al. 2000; Moreno et al. 2013; Patton et al. 2016; Ventou et al. 2019). The measured galaxies are located at projected distance from the targets of about 20−700 kpc (see Fig. 6). Those that are found associated with the targets ($\Delta V <$ 1000 km s$^{-1}$) are in the range from 50 to 500 kpc. The luminosity of the observed galaxies spreads over a wide range from $M(r) = -17$ to $M(r) = -22$, while those that are found at the same redshift of the targets cover the higher luminosity range [on average $M(r) = -21.2$] (see Fig. 7). The average number of galaxies detected within 0.25 Mpc of the quasar for our observed 12 QSO fields is 19 ± 6, while that for the 11 inactive galaxies fields is 18 ± 8 (Karhunen et al. 2014). The same similarity is found for the galaxy number density that is 7 ± 2 ($N_{\rm gal}$ arcmin$^{-2}$) for the 12 QSO fields and 7 ± 3 ($N_{\rm gal}$ arcmin$^{-2}$) for the galaxy fields (Karhunen et al. 2014).

We found that 5 out of 12 observed fields of quasars exhibit at least one companion galaxy and in three cases more than one companion was found. One companion galaxy was found in 3 out of 11 ING fields. The projected separations and the luminosity of companion galaxies of quasars are similar to those of ING. Also, the incidence of companions does not appear significantly different (albeit with scanty statistics) between QSO and ING. In Table 3, we list the data for all the companion galaxies.

As far as the SF signature of the associated companions is concerned, we found that for QSO only one companion galaxy exhibits [O II] and/or [O III] emission lines. On the contrary, none of the three companions of ING show emission lines.[1]

### 4.1 Extended analysis from SDSS data

In addition to our spectroscopic observations, we also search for companion galaxies using the SDSS DR16 (Ahumada et al. 2020) data base and using the same conditions for companion selection as described above. In particular, we searched the SDSS spectroscopic data base for companion galaxies in the fields of the 416 QSOs (Falomo et al. 2014) and of 580 passive galaxies (Karhunen et al. 2014).

This search resulted in 267 QSO fields (∼64 per cent of the full sample) with at least one galaxy with spectrum and 434 for the ING fields (∼75 per cent of the full sample).

Applying the same conditions as described in Section 4 for the projected distance and the velocity difference from the target, we found 58 companion galaxies in 46 QSO fields. For 34 of them, at least one companion galaxy was found. The average absolute magnitude of these companions is $<M_r> = -21.5 \pm 0.9$. For the ING, we found 99 companion galaxies in 84 fields. For 62 ING, at least one companion galaxy was found and for the remaining fields more than one companion was found. The average absolute magnitude of all these companions is $<M_r> = -21.8 \pm 0.8$. The distribution of absolute magnitude is similar for the two samples (see Fig. 8).

[1]Note that one of the fields of quasars (QSO 192) was already known to have companions; therefore, the effective number of companions of quasars is 4 out of 11 objects.

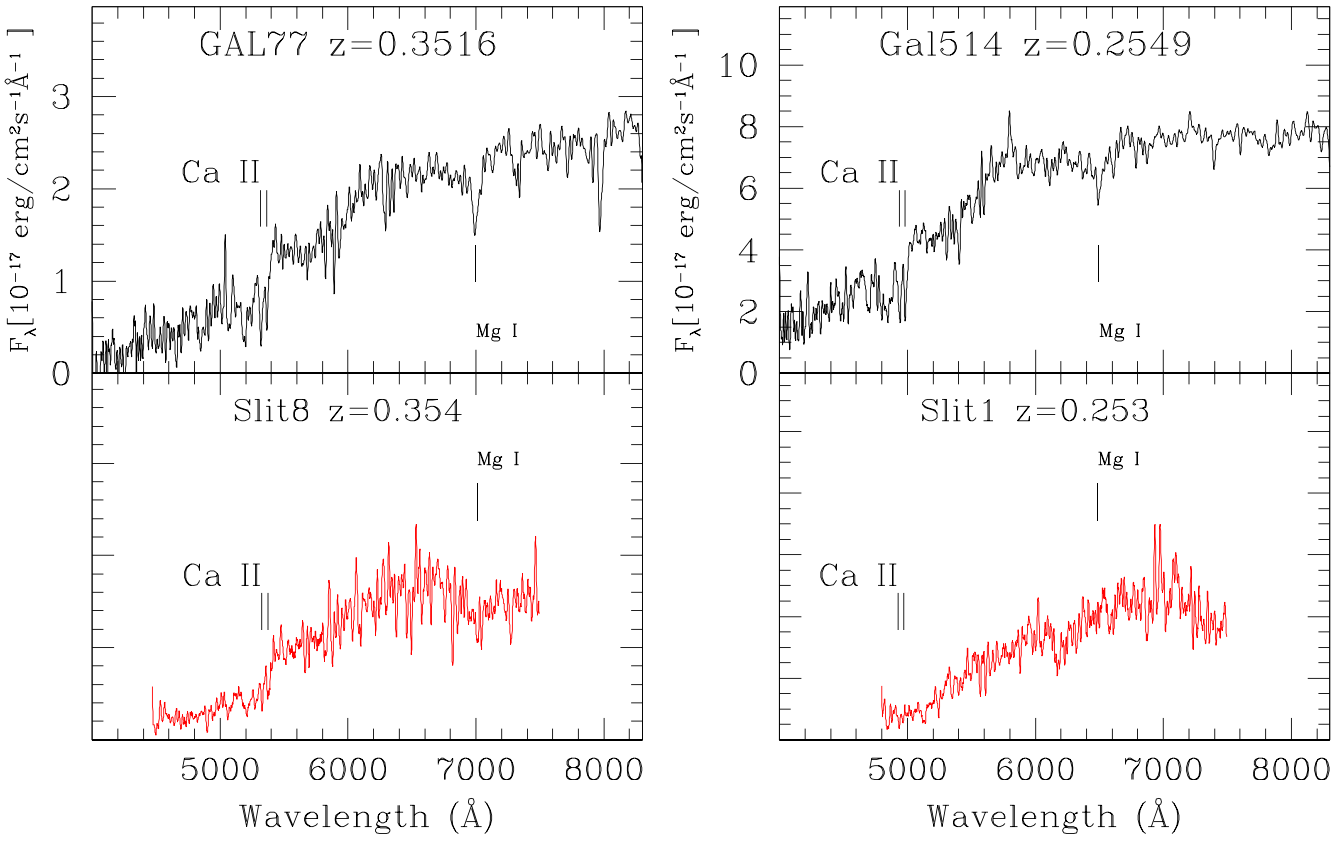


**Figure 5.** Examples of the optical spectrum of the inactive galaxies (top panels) from SDSS DR16 and the companion galaxy (bottom panels) from this work. Galaxy numbers are taken from Karhunen et al. (2014).

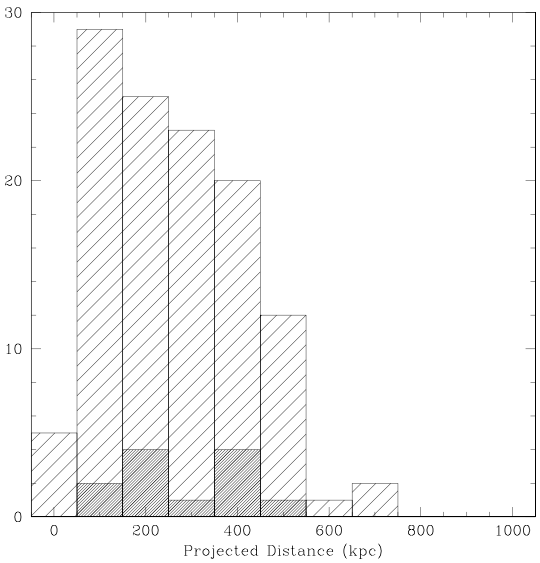


**Figure 6.** Distribution of the projected distance (in Kpc) from the main target for observed galaxies in the fields of QSO and ING. The galaxies not associated (different redshift) with the targets are shown by shaded area, while those associated (see text) are represented by filled area.

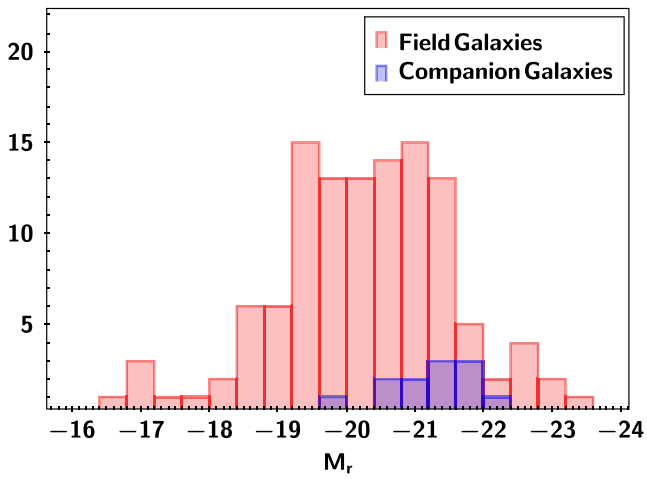


**Figure 7.** Distribution of $M_r$ absolute magnitude of field and associated companion galaxies observed in this work.

The incidence of companions (number of objects that have at least one companion galaxy) appears similar for the two samples: 17 per cent for QSO and 19 per cent for ING. The incidence of companions of QSO from SDSS data set is significantly lower than that found in our data set (∼40 per cent). Considering that the objects with SDSS spectra might be chosen somewhat differently from the various fields, we believe that the difference of incidence of QSO companions is mainly dependent on the selection of the spectroscopic targets (long slit/MOS and fibres). In fact, the distribution of the projected distance of companions is significantly different between our sample (<PD> = 132 kpc) and SDSS data set (<PD> = 502 kpc). The incidence of QSO companions at PD < 500 kpc for SDSS data set is ∼25 per cent.

**Table 3.** Properties of companion galaxies from MOS observations.

| ID | Slit ID | SDSS | $z$ | PD (kpc) | $M_r$ | $\Delta V$ (km s$^{-1}$) |
|---|---|---|---|---|---|---|
| QSO-192 | 4 | J002834.72−000424.3 | 0.252 | 183 | −21.37 | 50 |
| | 10 | J002825.26−000319.8 | 0.249 | 431 | −21.03 | 869 |
| GAL-35 | 4 | J002904.22−002850.0 | 0.291 | 189 | −20.8 | 120 |
| QSO-205 | 3 | J004324.47+005223.5 | 0.309 | 447 | −20.53 | 210 |
| | 4 | J004322.78+005153.8 | 0.307 | 270 | −21.6 | 390 |
| GAL-77 | 8 | J010537.57+005305.8 | 0.354 | 434 | −22.08 | 720 |
| QSO-62 | 3 | J215744.50+005400.7 | 0.266 | 235 | −21.72 | 420 |
| GAL-514 | 1 | J223002.81+000319.4 | 0.253 | 447 | −21.51 | 570 |
| QSO-127 | 4 | J231253.23+001715.9 | 0.258 | 142 | −20.89 | 300 |
| | 5 | J231252.38+001754.5 | 0.26 | 169 | −19.87 | 899 |
| | 11 | J231243.31+001822.5 | 0.257 | 520 | −21.58 | 50 |
| QSO-154 | 5 | J234933.10−003645.2 | 0.28 | 55 | −21.64 | 300 |

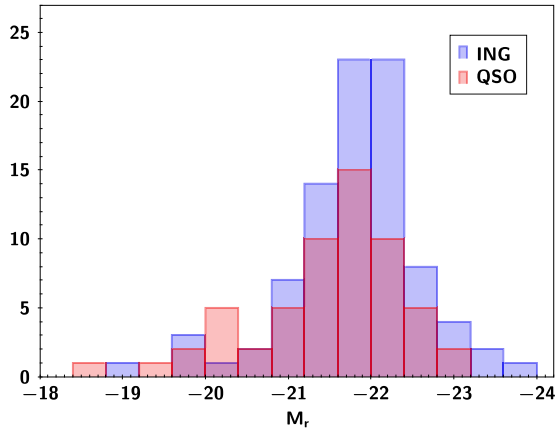


**Figure 8.** Distribution of $M_r$ absolute magnitudes of associated companion galaxies for both QSO and ING from the extended sample derived from SDSS DR16.

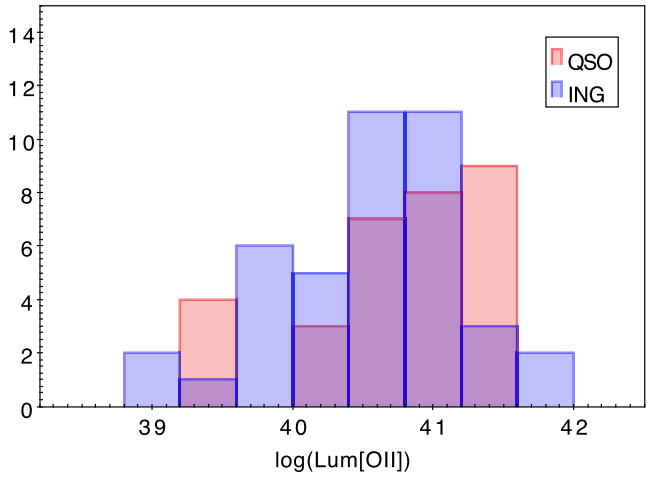


**Figure 9.** Distribution of the [O II] 3727 Å luminosity of associated companion galaxies for both QSO and ING derived from SDSS database. The two distributions are not significantly different (see text).

## 5 DISCUSSION

Combining our new results with those from Paper I and Paper II, we can investigate the close environment properties of 44 low-$z$ QSOs by obtaining spectroscopy of the companion objects in their fields and probe physical association and possible events of recent SF. For about half (19 out of 44) of the observed QSOs, we found at least one associated companion galaxy and in few cases more than one associated companion is found. In this whole sample, we found 28 companion galaxies.

In order to better characterize the companion galaxies of QSO, we evaluated the stellar mass of the 27 companions from our full sample of 44 QSO fields using equation (1) in Gilbank et al. (2010), $\log_{10}(M_\star/M_\odot) = 0.480(g-r)_0 - 0.475M_z - 0.08$ (see also Paper II). We found the average stellar mass is $< \log(M_\star/M_\odot) > = 10.6 \pm 0.8$. Similarly for the 58 companions found for 46 QSO fields using the SDSS spectroscopic data (see Section 4.1), we found the average stellar mass is $< \log(M_\star/M_\odot) > = 11.3 \pm 0.7$. A moderately higher mass for the SDSS companions is expected since these companions are on average somewhat more luminous than those found in our sample [$<M(R)> = -21.8$ for SDSS companions and $<M(R)> = -20.9$ for our sample]. This is likely an observational effect because of the higher average redshift for the SDSS data ($<z> = 0.35$ with respect to $<z> = 0.26$). In fact, the spectroscopy of companion galaxies from SDSS data was secured for targets on average ∼1 magnitude brighter than the companions in our sample. This translates into more luminous objects and consequently also more massive.

Of the 19 QSOs with at least one companion, 14 of them show [O II] emission lines as possible signature of recent SF. The average [O II] luminosity for these companions is $<\log(L(\mathrm{O\,II})> = 41.02 \pm 0.6$ erg s$^{-1}$.

We also searched for [O II] emission line in the companion galaxies of QSO and ING from SDSS spectroscopic data base (see also Section 4.1). For the 58 companions of QSO, we found spectral line measurements in SDSS data set only for 33 objects. For the remaining 25 sources, we retrieved the spectra and search for [O II] emission line. We got flux measurements of the [O II] line for 31 companion galaxies (i.e. the 53 per cent of the whole companion sample). We then performed a similar search for the 99 companions of ING. Also, in this case, we found SDSS spectroscopic measurements only for 68 objects and for the other 31 we inspected their spectrum to search for [O II] line. For ING, there are 41 companions with [O II] line measured (i.e. 41 per cent of the whole companion sample).

Finally, from these flux measurements, we computed the [O II] 3727Å line luminosity. We find that the distribution of the [O II] luminosity is not significantly different for companions of QSO and of ING (see Fig. 9). The average line luminosity is $<\log(L[\mathrm{O\,II}])> = (40.76 \pm 0.6)$ erg s$^{-1}$ and $<\log(L[\mathrm{O\,II}])> = (40.49 \pm 0.6)$ erg s$^{-1}$ for QSO and ING companions, respectively. For both QSO and

ING companions, there are few objects with a particularly high SFR (SFR $> 15\ M_{\odot}\ \mathrm{yr}^{-1}$). Excluding these outliers, the two distributions are similar showing a concentration of values at SFR $< 4\ M_{\odot}\ \mathrm{yr}^{-1}$. On average, SFR (QSO companions) $= 4.9 \pm 4.0\ M_{\odot}\ \mathrm{yr}^{-1}$ and SFR (ING companions) $= 3.2 \pm 2.6\ M_{\odot}\ \mathrm{yr}^{-1}$; this is comparable to the value ($4.3\ M_{\odot}\ \mathrm{yr}^{-1}$) found for the QSO companions in Paper II.

This confirms our previous results (Paper II) based on long-slit spectroscopy of 34 QSO fields. In spite of the scanty statistics, the comparison of galaxies in the fields of QSO with those of ING does not show significant differences for the incidence of close companions and/or for their global properties at low redshift. This is also consistent with the results derived from the analysis of spectroscopic data from SDSS data base although, in this case, the incidence of companions is smaller likely due to the small number of available spectra in the fields of QSO and ING. However, the signature of recent SF given by the presence of emission lines of the QSO companions supports a modest link between the nuclear activity and SF in the environments.

Our overall results differ from the finding of Ellison et al. (2011), who report a higher incidence of close (<80 kpc) companions for a larger selection of lower redshift (<0.2) AGNs with respect to a control sample of galaxies without companions. The higher incidence is enhanced for smaller projected separations. This suggests that the effect of companions on nuclear activity and triggering of recent SF might be relevant only for very small physical separation of the companion from the galaxy.

Given the significance of the topic for the investigation of the impact of the environments on the nuclear activity, it is important to extend this study to larger samples of QSO and ING with very similar characteristics of QSO host galaxies. The use of larger telescopes would also allow one to use a sample of objects at higher redshift and thus probe whether there is some evolution with the cosmic time. We plan to extend this programme in the near future.

## ACKNOWLEDGEMENTS

We thank the anonymous referee whose comments improved the paper. This work is based on observations collected at the ESO under ESO programme(s) 0103.B-0737 and 0104.B-0197. MBS acknowledges funding from the Finnish Cultural Foundation and Finnish Centre for Astronomy; (FINCA). MBS and JKK acknowledge financial support from the Academy of Finland, grant 311438.

Funding for the Sloan Digital Sky Survey, SDSS-IV has been provided by the Alfred P. Sloan Foundation, the U.S. Department of Energy Office of Science, and the participating institutions. SDSS-IV acknowledges support and resources from the Center for High-Performance Computing at the University of Utah. The SDSS web site is www.sdss.org.

SDSS-IV is managed by the Astrophysical Research Consortium for the participating institutions of the SDSS Collaboration, including the Brazilian Participation Group, the Carnegie Institution for Science, Carnegie Mellon University, the Chilean Participation Group, the French Participation Group, Harvard-Smithsonian Center for Astrophysics, Instituto de Astrofísica de Canarias, The Johns Hopkins University, Kavli Institute for the Physics and Mathematics of the Universe (IPMU)/University of Tokyo, the Korean Participation Group, Lawrence Berkeley National Laboratory, Leibniz Institut für Astrophysik Potsdam (AIP), Max-Planck-Institut für Astronomie (MPIA Heidelberg), Max-Planck-Institut für Astrophysik (MPA Garching), Max-Planck-Institut für Extraterrestrische Physik (MPE), National Astronomical Observatories of China, New Mexico State University, New York University, University of Notre Dame, Observatário Nacional/MCTI, The Ohio State University, Pennsylvania State University, Shanghai Astronomical Observatory, United Kingdom Participation Group, Universidad Nacional Autónoma de México, University of Arizona, University of Colorado Boulder, University of Oxford, University of Portsmouth, University of Utah, University of Virginia, University of Washington, University of Wisconsin, Vanderbilt University, and Yale University.

## DATA AVAILABILITY

The data underlying this article are available through the ESO archive at http://archive.eso.org and can be accessed with proposal IDs 0103.B-0737 and 0104.B-0197.

## REFERENCES

Ahumada R. et al., 2020, ApJS, 249, 3
Annis J. et al., 2014, ApJ, 794, 120
Bettoni D., Falomo R., Kotilainen J. K., Karhunen K., Uslenghi M., 2015, MNRAS, 454, 4103
Bettoni D., Falomo R., Kotilainen J. K., Karhunen K., 2017, MNRAS, 466, 3600 (Paper I)
Di Matteo T., Springel V., Hernquist L., 2005, Nature, 433, 604
Ellison S. L., Patton D. R., Mendel J. T., Scudder J. M., 2011, MNRAS, 418, 2043
Falomo R., Bettoni D., Karhunen K., Kotilainen J. K., Uslenghi M., 2014, MNRAS, 440, 476
Ferrarese L., Merritt D., 2000, ApJ, 539, L9
Freudling W., Romaniello M., Bramich D. M., Ballester P., Forchi V., García-Dabló C. E., Moehler S., Neeser M. J., 2013, A&A, 559, A96
Gilbank D. G., Baldry I. K., Balogh M. L., Glazebrook K., Bower R. G., 2010, MNRAS, 405, 2594
Jacoby G. H., Hunter D. A., Christian C. A., 1984, ApJS, 56, 257
Karhunen K., Kotilainen J. K., Falomo R., Bettoni D., 2014, MNRAS, 441, 1802
Kauffmann G., Haehnelt M., 2000, MNRAS, 311, 576
Kormendy J., Ho L. C., 2013, ARA&A, 51, 511
Kurtz M. J., Mink D. J., 1998, PASP, 110, 934
Moreno J., Bluck A. F. L., Ellison S. L., Patton D. R., Torrey P., Moster B. P., 2013, MNRAS, 436, 1765
Patton D. R., Carlberg R. G., Marzke R. O., Pritchet C. J., da Costa L. N., Pellegrini P. S., 2000, ApJ, 536, 153
Patton D. R., Qamar F. D., Ellison S. L., Bluck A. F. L., Simard L., Mendel J. T., Moreno J., Torrey P., 2016, MNRAS, 461, 2589
Serber W., Bahcall N., Ménard B., Richards G., 2006, ApJ, 643, 68
Shanks T., Tanvir N. R., Redfern M., 1988, PASP, 100, 1226
Shen Y. et al., 2009, ApJ, 697, 1656
Smith R. J., Lucey J. R., Hudson M. J., Schlegel D. J., Davies R. L., 2000, MNRAS, 313, 469
Stone M. B., Bettoni D., Falomo R., Kotilainen J. K., Karhunen K., Paiano S., Scarpa R., 2021, MNRAS, 501, 419 (Paper II)
Stott J. P. et al., 2020, MNRAS, 497, 3083
Strand N. E., Brunner R. J., Myers A. D., 2008, ApJ, 688, 180
Ventou E. et al., 2019, A&A, 631, A87
Wake D. A. et al., 2004, ApJ, 610, L85
Wethers C. F. et al., 2022, ApJ, 928, 192
Wijesinghe D. B. et al., 2012, MNRAS, 423, 3679

## APPENDIX A: GALAXIES IN THE FIELD OF QUASARS

**Table A1.** Observed galaxies.

| ID | Slit ID | SDSS | RA (2000) | Dec. (2000) | $m_r$ | PD kpc | $M_r$ | $z$ |
|---|---|---|---|---|---|---|---|---|
| GAL-32 | 3 | J002430.92+000718.1 | 6.128858 | 0.121712 | 19.25 | 349 | − 22.69 | 0.44 |
| | 4 | J002430.91+000744.5 | 6.128801 | 0.129055 | 19.47 | 177 | − 21.47 | 0.299 |
| | 6 | J002437.66+000840.7 | 6.156919 | 0.144652 | 18.75 | 337 | − 22.08 | 0.285 |
| | 8 | J002437.22+000929.1 | 6.155118 | 0.15809 | 19.15 | 352 | − 20.97 | 0.214 |
| QSO-192A | 3 | J002835.69−000308.1 | 7.14875 | − 0.052264 | 21.07 | 337 | − 19.34 | 0.241 |
| | 4 | J002834.72−000424.3 | 7.144705 | − 0.073424 | 19.15 | 183 | − 21.37 | 0.252 |
| | ∗6 | J002831.36−000409.8 | 7.13069 | − 0.069405 | 18.75 | – | – | – |
| | 7 | J002829.81−000311.3 | 7.124212 | − 0.05314 | 19.05 | 241 | − 21.12 | 0.218 |
| | 8 | J002828.98−000333.1 | 7.120756 | − 0.059209 | 19.25 | 202 | − 20.91 | 0.218 |
| | 9 | J002826.55−000258.5 | 7.110658 | − 0.049595 | 21.3 | 488 | − 19.72 | 0.308 |
| | 10 | J002825.26−000319.8 | 7.105283 | − 0.055525 | 19.46 | 431 | − 21.03 | 0.249 |
| QSO-192B | 3 | J002835.57−000544.7 | 7.148225 | − 0.095774 | 19.6 | 673 | − 22.75 | 0.517 |
| | 4 | J002834.47−000452.6 | 7.143654 | − 0.081303 | 20.74 | 362 | − 22.41 | 0.229 |
| | 5 | J002832.86−000446.7 | 7.136934 | − 0.07964 | 20.26 | 132 | − 19.9 | 0.218 |
| | 7 | J002829.37−000248.6 | 7.122386 | − 0.046845 | 21.56 | 326 | − 18.63 | 0.22 |
| | 8 | J002828.72−000341.7 | 7.119697 | − 0.061607 | 18.73 | 193 | − 21.43 | 0.218 |
| | ∗10 | J002824.70−000453.8 | 7.10293 | − 0.081622 | 17.51 | – | – | – |
| GAL-35 | 4 | J002904.22−002850.0 | 7.267615 | − 0.480557 | 20.08 | 189 | − 20.8 | 0.291 |
| | 7 | J002900.06−002825.8 | 7.250284 | − 0.47386 | 18.03 | 68 | − 21.49 | 0.167 |
| | 8 | J002858.12−002730.8 | 7.242195 | − 0.458572 | 20.32 | 345 | − 20.49 | 0.283 |
| | 9 | J002856.44−002723.1 | 7.235168 | − 0.45644 | 19.78 | 485 | − 21.35 | 0.321 |
| | 10 | J002854.14−002815.1 | 7.225603 | − 0.470888 | 21.38 | 454 | − 19.21 | 0.259 |
| QSO-195 | 2 | J003438.06−001301.1 | 8.658602 | − 0.216976 | 19.36 | 465 | − 21.92 | 0.342 |
| | 4 | J003435.29−001401.0 | 8.647048 | − 0.233638 | 19.0 | 281 | − 21.5 | 0.249 |
| | 7 | J003431.17−001306.4 | 8.629897 | − 0.218455 | 20.83 | 51 | − 20.42 | 0.338 |
| | 9 | J003428.43−001326.4 | 8.618481 | − 0.224004 | 19.11 | 146 | − 20.39 | 0.165 |
| GAL-45 | 6 | J004045.79+000848.6 | 10.190822 | 0.146835 | 20.61 | 45 | − 20.05 | 0.267 |
| | 8 | J004049.02+000833.9 | 10.204253 | 0.142758 | 21.13 | 225 | − 19.28 | 0.241 |
| QSO-204 | 5 | J004215.17+005904.7 | 10.563217 | 0.984665 | 19.51 | 119 | − 21.18 | 0.27 |
| | 6 | J004213.73+005804.9 | 10.55725 | 0.968047 | 20.15 | 172 | − 18.83 | 0.133 |
| | 7 | J004212.89+005905.2 | 10.553716 | 0.984802 | 20.37 | 82 | − 21.33 | 0.403 |
| | 8 | J004211.54+005739.3 | 10.548116 | 0.960936 | 18.44 | 515 | − 22.97 | 0.359 |
| QSO-205A | 1 | J004327.59+005009.5 | 10.864977 | 0.835977 | 21.06 | 705 | − 20.51 | 0.382 |
| | 3 | J004324.47+005223.5 | 10.851991 | 0.873201 | 20.5 | 448 | − 20.53 | 0.309 |
| | 4 | J004322.78+005153.8 | 10.844932 | 0.864971 | 19.41 | 270 | − 21.6 | 0.307 |
| | 6 | J004320.54+005059.9 | 10.8356 | 0.849998 | 20.1 | 67 | − 19.95 | 0.208 |
| | 7 | J004318.07+005117.2 | 10.825316 | 0.854799 | 20.39 | 116 | − 20.72 | 0.318 |
| | 9 | J004314.63+005138.3 | 10.810969 | 0.860662 | 20.47 | 190 | − 18.53 | 0.134 |
| QSO-205B | 1 | J004326.98+005243.8 | 10.862419 | 0.878852 | 22.2 | 360 | − 17.01 | 0.147 |
| | 2 | J004325.80+005125.6 | 10.857539 | 0.857129 | 22.04 | 327 | − 18.15 | 0.221 |
| | 3 | J004324.33+005127.8 | 10.851384 | 0.85774 | 21.63 | 133 | − 16.75 | 0.103 |
| | 6 | J004319.77+005155.0 | 10.832392 | 0.865293 | 20.52 | 136 | − 19.56 | 0.21 |
| GAL-55 | 2 | J005029.39−002211.5 | 12.622493 | − 0.369876 | 20.31 | 324 | − 20.06 | 0.237 |
| | 3 | J005027.76−002400.6 | 12.615691 | − 0.400179 | 20.37 | 389 | − 20.74 | 0.319 |
| | 5 | J005025.06−002318.7 | 12.604427 | − 0.388548 | 19.17 | 77 | − 20.39 | 0.315 |
| | 6 | J005023.83−002224.9 | 12.599326 | − 0.373584 | 20.37 | 120 | − 20.18 | 0.255 |
| | 7 | J005022.28−002238.6 | 12.592871 | − 0.377411 | 21.39 | 116 | − 18.55 | 0.199 |
| | ∗8 | J005019.91−002322.4 | 12.58298 | − 0.389557 | 15.32 | – | – | – |
| GAL-76 | 1 | J010517.21+005203.3 | 16.321709 | 0.867587 | 19.98 | 424 | − 20.49 | 0.246 |
| | 2 | J010513.92+005228.5 | 16.308042 | 0.874592 | 21.3 | 418 | − 19.52 | 0.284 |
| | 3 | J010515.37+005238.8 | 16.31406 | 0.877458 | 21.09 | 298 | − 19.31 | 0.24 |
| | 4 | J010515.22+005308.5 | 16.313437 | 0.885696 | 21.17 | 179 | − 18.86 | 0.206 |
| | 5 | J010521.32+005319.1 | 16.338868 | 0.888654 | 20.64 | 207 | − 18.95 | 0.172 |
| | ∗7 | J010515.78+005423.8 | 16.31575 | 0.906617 | 17.95 | – | – | – |
| | 8 | J010517.29+005444.0 | 16.322064 | 0.912239 | 19.1 | 202 | − 21.43 | 0.253 |
| | 9 | J010516.81+005458.5 | 16.320042 | 0.916264 | 19.93 | 197 | − 19.72 | 0.176 |
| | 10 | J010513.59+005529.7 | 16.306626 | 0.92494 | 20.35 | 357 | − 19.53 | 0.194 |
| GAL-77 | 1 | J010550.20+005308.2 | 16.459191 | 0.885623 | 20.5 | 488 | − 20.67 | 0.327 |
| | 3 | J010546.93+005313.4 | 16.445542 | 0.887064 | 20.15 | 244 | − 20.86 | 0.307 |
| | 5 | J010543.84+005300.9 | 16.43268 | 0.883587 | 19.63 | 64 | − 20.73 | 0.236 |
| | 8 | J010537.57+005305.8 | 16.406576 | 0.884954 | 19.3 | 434 | − 22.08 | 0.354 |

**Table A1** – *continued*

| ID | Slit ID | SDSS | RA (2000) | Dec. (2000) | $m_r$ | PD kpc | $M_r$ | $z$ |
|---|---|---|---|---|---|---|---|---|
| GAL-80 | 4 | J010611.40−001939.1 | 16.54751 | −0.327541 | 20.19 | 151 | −21.11 | 0.343 |
| | 5 | J010615.18−001912.1 | 16.563272 | −0.320034 | 19.45 | 220 | −21.34 | 0.28 |
| | 6 | J010611.51−001850.4 | 16.547963 | −0.314 | 18.76 | 54 | −20.81 | 0.17 |
| | 7 | J010611.25−001821.8 | 16.546884 | −0.30606 | 19.47 | 137 | −20.09 | 0.169 |
| GAL-81 | 3 | J010616.20+005515.1 | 16.567531 | 0.92088 | 19.39 | 287 | −21.2 | 0.258 |
| | 4 | J010608.49+005550.4 | 16.535408 | 0.930693 | 18.18 | 402 | −23.31 | 0.371 |
| | 6 | J010609.71+005641.4 | 16.540485 | 0.944856 | 19.18 | 240 | −21.25 | 0.242 |
| | 8 | J010611.27+005720.5 | 16.546962 | 0.955698 | 19.15 | 256 | −20.94 | 0.211 |
| QSO-239A | 2 | J012054.02−001942.1 | 20.22509 | −0.328372 | 21.52 | 292 | −18.63 | 0.217 |
| | 3 | J012050.51−001919.5 | 20.210488 | −0.322097 | 20.77 | 173 | −19.53 | 0.23 |
| | 3 | J012050.51−001919.5 | 20.210487 | −0.322097 | 20.77 | 376 | −20.35 | 0.323 |
| | 4 | J012049.56−001849.0 | 20.206527 | −0.313618 | 21.66 | 96 | −18.62 | 0.229 |
| | 5 | J012050.27−001829.4 | 20.209467 | −0.308185 | 19.73 | 52 | −21.56 | 0.342 |
| | 6 | J012050.84−001820.7 | 20.211846 | −0.305758 | 19.12 | 49 | −21.41 | 0.253 |
| | 8 | J012051.73−001733.4 | 20.215565 | −0.29262 | 20.28 | 157 | −18.95 | 0.148 |
| | 9 | J012051.28−001712.4 | 20.213697 | −0.286787 | 18.68 | 174 | −20.06 | 0.12 |
| | 10 | J012055.53−001653.8 | 20.231412 | −0.281628 | 19.37 | 470 | −21.11 | 0.248 |
| QSO-239B | 1 | J012055.05−002011.6 | 20.229396 | −0.336566 | 20.42 | 384 | −19.54 | 0.2 |
| | 2 | J012053.83−001926.9 | 20.224309 | −0.324165 | 19.49 | 251 | −20.76 | 0.226 |
| | 4 | J012051.32−001844.9 | 20.213844 | −0.312487 | 20.74 | 52 | −19.79 | 0.252 |
| | 6 | J012052.51−001819.3 | 20.218821 | −0.305365 | 20.91 | 101 | −19.43 | 0.233 |
| | 7 | J012055.53−001740.6 | 20.231381 | −0.294636 | 20.48 | 337 | −20.01 | 0.249 |
| | 8 | J012045.29−001714.3 | 20.188725 | −0.287309 | 19.02 | 591 | −22.45 | 0.369 |
| | 9 | J012055.53−001653.8 | 20.231412 | −0.281628 | 19.37 | 470 | −21.12 | 0.249 |
| GAL-120 | 4 | J014651.96+001218.5 | 26.716505 | 0.205162 | 20.12 | 43 | −19.77 | 0.194 |
| | 5 | J014652.66+001231.8 | 26.719458 | 0.208836 | 20.32 | 17 | −17.32 | 0.075 |
| QSO-270 | 2 | J015243.47+000832.5 | 28.181137 | 0.142384 | 20.89 | 369 | −19.67 | 0.256 |
| | ∗3 | J015242.48+000750.1 | 28.177038 | 0.130607 | 19.43 | – | – | – |
| | 6 | J015237.44+000832.1 | 28.156018 | 0.142255 | 18.66 | 278 | −22.03 | 0.269 |
| | 8 | J015233.45+000933.7 | 28.139416 | 0.159375 | 20.17 | 305 | −20.16 | 0.233 |
| | 1 | J015245.20+000940.9 | 28.188347 | 0.161374 | 21.15 | 456 | −20.11 | 0.339 |
| | 2 | J015243.68+000853.0 | 28.182022 | 0.148076 | 20.3 | 382 | −20.78 | 0.315 |
| | 5 | J015238.62+000858.6 | 28.160924 | 0.149639 | 21.05 | 92 | −18.05 | 0.14 |
| | ∗8 | J015232.47+001102.4 | 28.13532 | 0.184005 | 20.52 | – | – | – |
| QSO-16 | ∗1 | J205002.39−001158.0 | 312.5099 | −0.19945 | 18.49 | – | – | – |
| | 3 | J204959.77−001042.1 | 312.499056 | −0.178361 | 20.13 | 454 | −21.18 | 0.345 |
| | 4 | J204957.82−001135.8 | 312.490936 | −0.193282 | 19.76 | 109 | −20.34 | 0.212 |
| | ∗7 | J204953.28−001219.3 | 312.472 | −0.20536 | 18.97 | – | – | – |
| | ∗9 | J204950.51−001032.4 | 312.46049 | −0.17568 | 17.15 | – | – | – |
| | 10 | J204949.21−001128.3 | 312.455045 | −0.191208 | 20.34 | 364 | −19.46 | 0.188 |
| QSO-62 | 1 | J215741.54+005448.4 | 329.423108 | 0.913448 | 20.44 | 398 | −19.75 | 0.22 |
| | ∗2 | J215743.40+005417.9 | 329.43084 | 0.90497 | 17.56 | – | – | – |
| | 3 | J215744.50+005400.7 | 329.435436 | 0.900209 | 18.94 | 235 | −21.72 | 0.266 |
| | 5 | J215744.26+005313.8 | 329.434427 | 0.887169 | 19.79 | 44 | −21.06 | 0.288 |
| | 9 | J215743.39+005139.8 | 329.430827 | 0.86108 | 19.37 | 419 | −21.98 | 0.351 |
| QSO-68 | ∗1 | J215955.74+000920.3 | 329.98228 | 0.15564 | 15.56 | – | – | – |
| | 2 | J215954.23+000947.5 | 329.975959 | 0.163198 | 21.17 | 340 | −19.61 | 0.28 |
| | 3 | J215953.15+000842.2 | 329.971459 | 0.145063 | 19.88 | 515 | −21.5 | 0.355 |
| | 4 | J215951.87+000949.6 | 329.966125 | 0.163793 | 20.02 | 180 | −20.53 | 0.254 |
| | 8 | J215946.16+000946.5 | 329.942337 | 0.162929 | 20.81 | 357 | −22.89 | 0.86 |
| GAL-514 | 1 | J223002.81+000319.4 | 337.511713 | 0.055415 | 19.02 | 447 | −21.51 | 0.253 |
| | 3 | J222959.39+000421.3 | 337.497473 | 0.072591 | 20.67 | 188 | −19.76 | 0.242 |
| | 5 | J222956.09+000354.7 | 337.483728 | 0.06521 | 20.79 | 62 | −19.22 | 0.205 |
| | ∗4 | J222957.80+000431.3 | 337.490863 | 0.075382 | 19.64 | – | – | – |
| | 6 | J222954.70+000452.6 | 337.477918 | 0.081287 | 20.98 | 105 | −17.95 | 0.13 |
| | ∗9 | J222950.41+000547.0 | 337.46005 | 0.096401 | 18.88 | – | – | – |
| | 10 | J222949.54+000254.5 | 337.456454 | 0.04849 | 20.52 | 396 | −19.27 | 0.187 |

**Table A1** *– continued*

| ID | Slit ID | SDSS | RA (2000) | Dec. (2000) | $m_r$ | PD kpc | $M_r$ | $z$ |
|---|---|---|---|---|---|---|---|---|
| QSO-127 | 2 | J231257.16+001643.9 | 348.238187 | 0.278865 | 19.26 | 459 | − 21.78 | 0.31 |
| | 4 | J231253.23+001715.9 | 348.221801 | 0.287771 | 19.7 | 142 | − 20.89 | 0.258 |
| | 5 | J231252.38+001754.5 | 348.21827 | 0.298477 | 20.74 | 169 | − 19.87 | 0.26 |
| | 7 | J231249.62+001751.0 | 348.206766 | 0.297515 | 20.82 | 182 | − 20.47 | 0.343 |
| | 8 | J231248.03+001839.0 | 348.200162 | 0.310856 | 19.04 | 305 | − 20.97 | 0.204 |
| | 11 | J231243.31+001822.5 | 348.180481 | 0.306263 | 19.0 | 520 | − 21.58 | 0.257 |
| GAL-548 | 1 | J232053.26−001943.3 | 350.221938 | − 0.328719 | 21.4 | 369 | − 18.93 | 0.233 |
| | 2 | J232054.49−001923.4 | 350.227065 | − 0.323177 | 18.37 | 238 | − 21.07 | 0.161 |
| | 3 | J232050.86−001901.8 | 350.211921 | − 0.317185 | 21.1 | 183 | − 18.66 | 0.184 |
| | 4 | J232051.79−001850.3 | 350.215795 | − 0.31398 | 20.47 | 162 | − 19.77 | 0.225 |
| | 4 | J232051.85−001844.8 | 350.216068 | − 0.312452 | 20.02 | 120 | − 17.1 | 0.06 |
| | 5 | J232051.20−001827.5 | 350.213358 | − 0.30764 | 20.62 | 80 | − 19.15 | 0.185 |
| | 6 | J232053.20−001803.3 | 350.221701 | − 0.300929 | 20.82 | 62 | − 19.45 | 0.228 |
| | 7 | J232051.45−001751.2 | 350.214379 | − 0.297556 | 21.0 | 80 | − 20.09 | 0.316 |
| | ∗8 | J232050.85−001731.8 | 350.21191 | − 0.29217 | 17.39 | – | – | – |
| | 9 | J232050.07−001652.8 | 350.208643 | − 0.281351 | 21.48 | 331 | − 19.27 | 0.275 |
| | 11 | J232053.54−001614.9 | 350.223102 | − 0.270816 | 19.92 | 450 | − 20.64 | 0.256 |
| QSO-147 | 2 | J234140.96−003930.4 | 355.420669 | − 0.658461 | 18.71 | 347 | − 21.97 | 0.268 |
| | 5 | J234142.76−003834.8 | 355.42818 | − 0.643011 | 20.51 | 123 | − 19.75 | 0.226 |
| | 6 | J234138.16−003808.2 | 355.409032 | − 0.635635 | 18.94 | 206 | − 21.73 | 0.268 |
| | 10 | J234143.23−003641.0 | 355.430157 | − 0.611413 | 20.69 | 339 | − 19.7 | 0.239 |
| QSO-154 | 3 | J234936.33−003538.1 | 357.401411 | − 0.593943 | 18.73 | 276 | − 21.14 | 0.192 |
| | 5 | J234933.10−003645.2 | 357.38794 | − 0.612579 | 19.12 | 54 | − 21.64 | 0.28 |
| | 8 | J234926.74−003614.1 | 357.361437 | − 0.603933 | 19.56 | 359 | − 20.79 | 0.236 |
| | 9 | J234925.54−003753.1 | 357.356445 | − 0.631443 | 21.54 | 251 | − 16.94 | 0.107 |

*Notes.* Column 1: catalogue identification number from Falomo et al. (2014). Column 2: slit identification; an asterisk indicates that the object measured turned out to be a star. Column 3: SDSS identifier. Column 4: object RA. Column 5: object Dec. Column 6: apparent $r$ magnitude. Column 7: projected distance from the QSO/ING in kpc. Column 8: absolute $r$ magnitude. Column 9: measured redshift.

This paper has been typeset from a TEX/LATEX file prepared by the author.